energies

MDPI

Article

Computational Fluid Dynamics Analysis and Validation with Field Test of 1 MW Hydropower Turbine System

Ki-Ha Kim [1], Dong-Hyun Kim [1,*], Suk-Jin Hong [1] and Sang-Myung Lee [2]

[1] Graduate School of Mechanical and Aerospace Engineering, Gyeongsang National University, Jinju 52828, Republic of Korea
[2] Korea South-East Power Co. (KOEN), Jinju 52852, Republic of Korea
* Correspondence: dhk0521@gmail.com or dhk@gnu.ac.kr

Abstract: This study analyzed and validated a 1 MW hydropower turbine system using computational fluid dynamics (CFD) in conjunction with field test data. The fluid domain of the hydropower system includes the runner blade, vane, duct, and both inflow and outflow free surface flows. An implicit unsteady flow solver and the SST k-ω turbulence model were employed. The rotational motion of the rotor blade was simulated using the moving reference frame (MRF) method. To handle a non-conformal mesh among the intake, runner, and outlet domains, an internal interface boundary condition was applied. System performance was evaluated by adjusting the guide vane opening ratio and the runner blade pitch angle. A free surface model was also developed to accurately represent the water level. The results show that the CFD analysis predicted the turbine's power output with a maximum deviation of 1.7% from field test measurements under different tide conditions. The numerical analysis also confirmed the influence of the runner blade pitch angle, with a 1° change in pitch angle leading to a 68 kW variation in power output. The accuracy of the CFD analysis was verified by comparing it to performance data from actual field tests.

Keywords: hydropower turbine; computational fluid dynamics (CFD); free surface; moving reference frame (MRF); runner blade; guide vane; field test

check for updates

Academic Editor: Helena M. Ramos

Received: 14 November 2024
Revised: 12 January 2025
Accepted: 24 January 2025
Published: 29 January 2025

Citation: Kim, K.-H.; Kim, D.-H.; Hong, S.-J.; Lee, S.-M. Computational Fluid Dynamics Analysis and Validation with Field Test of 1 MW Hydropower Turbine System. *Energies* **2025**, *18*, 628. https://doi.org/10.3390/en18030628

Copyright: © 2025 by the authors. Licensee MDPI, Basel, Switzerland. This article is an open access article distributed under the terms and conditions of the Creative Commons Attribution (CC BY) license (https://creativecommons.org/licenses/by/4.0/).

1. Introduction

In the pursuit of environmentally friendly and sustainable energy sources, hydropower turbines have emerged as a promising technology. A hydropower turbine transmits mechanical energy from the fluid flowing through the device to its functional elements (such as a runner or piston) or, alternatively, from these operative elements back to the fluid within. These systems harness the kinetic energy of water to generate electricity, often operating in remote, resource-rich locations. It is reported that ancient Greek civilizations were the first to apply hydropower for practical purposes over 2000 years ago. Most hydropower stations are situated along natural rivers, where dams are constructed across the river's course to create reservoirs for water retention. With an increasing focus on renewable energy, the accurate prediction and optimization of hydropower turbine performance have become crucial.

The importance of hydropower has grown significantly with the rise of intermittent renewable energy sources. As a reliable and continuous source of electricity, hydropower helps balance fluctuations in solar and wind energy production. However, experimental and numerical studies of full-scale turbines face several challenges.

Recent advancements in computational fluid dynamics (CFD) have significantly transformed the design and performance analysis of hydraulic turbines. While traditional

methods have relied heavily on experimental approaches, CFD provides a cost-effective, reliable, and versatile solution for evaluating turbine operations under various conditions. Key aspects include deriving performance characteristics, analyzing unsteady phenomena such as cavitation, and identifying losses. The integration of CFD with optimization techniques has also enabled enhanced hydraulic performance and improved operational efficiency. Despite these advantages, challenges remain, including the selection of robust models and boundary conditions to capture complex hydrodynamic phenomena accurately. This study aimed to critically evaluate CFD methodologies, highlight their practical utilities, and identify research gaps in the computational analysis of hydraulic turbines [1]. The use of computational fluid dynamics (CFD) has been pivotal in advancing the design and optimization of Kaplan turbines, offering a comprehensive understanding of both theoretical and practical aspects. Recent studies have emphasized the integration of CFD with optimization techniques to enhance hydraulic performance and operational efficiency. Key areas of focus include the detailed modeling of turbine components, validation of simulation results with experimental data, and the assessment of unsteady phenomena such as cavitation and flow-induced vibrations. This approach not only improves the accuracy of performance predictions but also reduces the time and cost associated with traditional experimental methodologies. The findings underscore the importance of CFD as a robust tool for achieving precise and efficient turbine design [2]. Since previous survey studies have already explored extensive data in these references, we herein introduce selected research cases that apply CFD to hydropower turbines.

Kaniecki et al. [3] demonstrated the application of CFD in analyzing Kaplan turbines, highlighting the importance of turbulence model selection for accurate predictions. The study focused on using CFD to determine cam curve characteristics and operating parameters, showcasing its potential as a cost-effective and reliable tool for turbine design and performance optimization, especially when experimental resources are limited. Akinyemi et al. [4] investigated the performance of a hydropower system employing paddle wheels and bottom fins through CFD simulations. The study demonstrated the effects of various design features, such as paddle shape and bottom fins, on energy generation efficiency, achieving up to a 20% improvement in power output. Additionally, their research incorporated economic analysis, highlighting the feasibility and cost effectiveness of the system in generating renewable energy. Liu et al. [5] conducted a comprehensive study on runner lifting-up (RLU) phenomena during load rejection transients in Kaplan turbines, a critical issue causing structural damage and operational instability. Using advanced 3D CFD simulations, the study revealed that RLU is driven by a downstream pumping effect caused by high rotational speeds coinciding with low discharge rates. The authors proposed and validated a piecewise guide-vane closing rule, effectively mitigating RLU by breaking the concurrence of these conditions. Peczkis et al. [6] conducted experimental and numerical studies on small Kaplan turbines, emphasizing the influence of blade number on turbine efficiency. The study demonstrated that five-bladed designs yielded higher efficiencies (up to 84%) compared to four-bladed designs under similar operating conditions. Using the SST k-ω turbulence model, the authors validated their numerical findings with experimental data, showcasing the precision of CFD in analyzing turbine performance. Iovănel et al. [7] conducted a comprehensive numerical simulation and experimental validation of a full-scale 10 MW Kaplan turbine prototype under transient operations. Their study focused on capturing complex phenomena such as rotating vortex ropes (RVR) in the draft tube during part-load conditions and assessing the influence of key factors like boundary conditions, mesh resolution, and blade geometry on simulation accuracy. Using the SST k-ω turbulence model, they achieved reasonable agreement between numerical predictions and experimental results for torque and pressure fluctuations.

The aim of the present study was to compare field analysis data on the power output of a hydropower turbine with experimental data obtained through CFD. This study emphasizes the predictive capability of CFD in assessing hydropower turbine performance. Over the past decade, CFD has evolved into a highly reliable and practical tool for evaluating fluid-flow machinery. When precisely calibrated, CFD simulations can lead to design improvements, reduced operational costs, and enhanced system reliability. This research presents the numerical simulation of a full-scale 1 MW hydropower turbine operating at a rotational speed of 141.7 RPM. The simulation utilized the shear–stress transport (SST) k-ω turbulence model. The SST k-ω model offers enhanced accuracy in predicting near-wall flows and separation phenomena, which are critical in the performance analysis of rotating turbine blades. By leveraging the hybrid properties of the k-ω and k-ε models, this approach ensures accurate predictions in the near-wall region (where k-ω is applied) and in the free stream region (where k-ε is applied). Additionally, the SST k-ω model requires less computational cost compared to large eddy simulation (LES) or direct numerical simulation (DNS), making it suitable for large-scale hydropower turbine analyses. Given the rotating blade motion and the presence of unsteady separation in the runner and guide vane, the SST k-ω model was deemed the most appropriate for this study [7]. The turbine's power output was calculated over different time periods at high and low tide levels, revealing an increase in power output during low tides and a relative decrease during high tides. Both aspects were addressed in this study: initially, on-site measurements of flow rate and power output were conducted on a hydropower turbine system, and subsequently, the commercial software STAR-CCM+ (v2210) was employed to replicate these real-world scenarios through simulations.

2. Computational Fluid Dynamic (CFD) Methodology

In this study, three-dimensional unsteady Reynolds-averaged Navier–Stokes equations were applied to analyze the flow and performance of the hydropower turbine system. The fundamental flow equations, derived from the integral form of the Navier–Stokes equations, are introduced here. These equations consist of the continuity and momentum equations [8–10], as follows:

$$\frac{d}{dt}\int_V \rho dV + \int_S \rho(v - v_b)\cdot dS = 0 \tag{1}$$

$$\begin{aligned}&\tfrac{d}{dt}\int_V \rho v dV + \int_S \rho(v - v_b)\otimes v dS\\ &= \int_S (T - pI)\cdot da + \int_V \rho b dV\end{aligned} \tag{2}$$

In these equations, ρ, V, and S represent fluid density, control volume (CV), and closed surface, respectively. v, v_g denotes the fluid velocity vector and the grid velocity vector, respectively. t is time, T is viscous stress tensor, and B is vector of all body forces, including gravity, user-defined body force, and body force due to rotation, among others. The viscous stress tensor is defined as follows:

$$T = \mu_{eff}\left[\nabla v + \nabla v^T - \frac{2}{3}(\nabla\cdot v)I\right] \tag{3}$$

where μ_{eff} denotes the effective dynamic viscosity of the fluid, and I is identity matrix. The segregated flow model solves the flow equations (one for each component of velocity and one for pressure) in a segregated manner. All simulations employed the semi-implicit method for pressure-linked equations (SIMPLE) algorithm, in which the linkage between the momentum and continuity equation is achieved through a predictor-corrector approach. A second-order upwind scheme was applied to the convection term, and for unsteady

simulations, a second-order central difference scheme was applied for temporal discretization. To model the turbulence in the fluid domain, the shear–stress transport (SST) k-ω turbulence model was employed. The primary motivation for selecting this model was its superior capability in accurately capturing near-wall turbulent flows and boundary layer separation, both of which are essential for analyzing the rotating runner blades and guide vanes of hydropower turbines. The SST k-ω model combines the benefits of the k-ω model for near-wall regions with the robustness of the k-ε model in free-stream regions, thereby ensuring accurate and stable results throughout the computational domain. This approach allows for an efficient trade-off between computational cost and prediction accuracy, particularly for high-Reynolds-number flows in large-scale hydropower turbine systems. A useful explanation of the SST k-omega theory can be also found in reference [11]. The present CFD model can provide reliable and physically accurate simulations of the complex flow field around the runner blade and guide vane. The corresponding author's application cases similar to the CFD technique applied in this paper can be found in references [12,13].

3. Simulation Technique

3.1. Fluid Domain Modeling

To achieve a precise performance analysis of a blade designed using three-dimensional CFD, it is essential to consider not only the blade but also the entire waterway shape, duct, and guide vane geometry in the flow analysis. Therefore, in this study, the CAD model includes the entire waterway, guide vane, and rotating blade, with a tip gap of approximately 3 mm relative to the inner surface of the shrouded duct, to ensure an accurate performance analysis.

Figure 1 shows the overall geometry of the hydropower turbine system, including the guide vane, runner blade, and duct with waterway shapes. In the current flow analysis, the effect of blade rotation was modeled using the moving reference frame (MRF) method, separating the rotational and stationary regions. The flow field around the runner blade was solved using a moving reference frame (MRF) to incorporate the rotational motion of the runner.

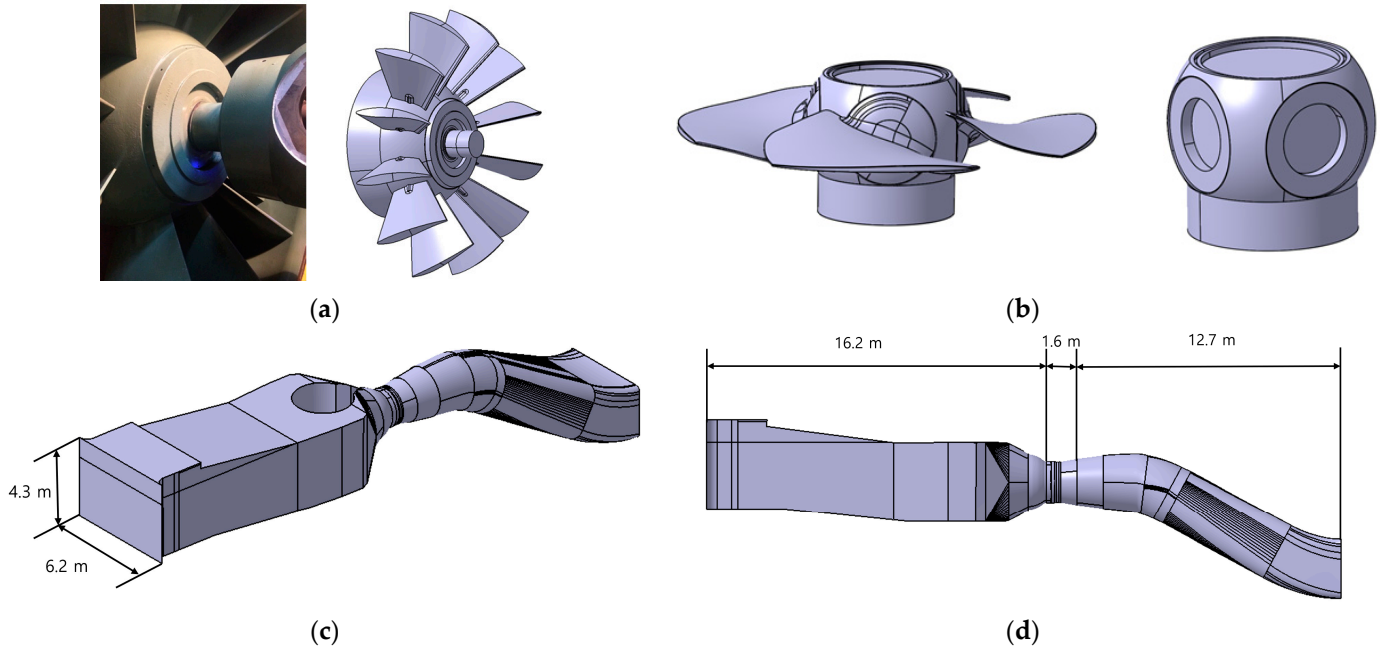


Figure 1. Geometry of the hydropower turbine system for CFD mesh domain: (**a**) guide vane; (**b**) runner blade and hub; (**c**) size of inlet part of hydropower turbine system; (**d**) side-view.

The MRF approach provides a flow solution for rotating machinery by applying a relative reference frame to the rotating domain. This method allows for a computationally efficient approach to model rotation, as it avoids the need for transient time-stepping required by the sliding mesh method. Unlike the sliding mesh method, which physically rotates the mesh at each time step to capture transient interactions between stationary and rotating domains, the MRF assumes a pseudo-steady-state condition where the reference frame rotates, while the mesh remains stationary. This approach provides a good balance between computational cost and accuracy, making it suitable for applications where transient interactions are not the primary focus. For instance, while the sliding mesh method offers higher fidelity in transient flow analyses, it demands significantly higher computational cost and time. The selection of MRF or sliding mesh depends on the specific objectives of the study. For steady-state analysis, the MRF approach is preferred due to its computational efficiency. However, if transient effects such as wake interaction or vortex shedding must be captured, the sliding mesh method becomes necessary. These distinctions are well established in prior studies, as discussed in Ferziger and Peric (2002) [10] and Versteeg and Malalasekera (2007) [14]. In addition, Abdelghany et al. [15] conducted a practical CFD performance analysis of rotating blades (wind turbine blades with winglets) under various conditions using the MRF (multiple reference frame) technique in ANSYS Fluent software.

There are two stationary regions and one rotational region. Consequently, the entire fluid domain is divided into a front inlet section (16.2 m) containing the guide vane, a central rotating section (1.6 m) containing the runner blade, and a rear outlet section (12.7 m) containing the draft tube. The inlet face measures 6.2 × 4.3 m, and the overall horizontal length of the fluid domain, excluding the outlet seawater field, is 30.5 m. Figure 2 illustrates the definition of the pitch angle for both the guide vane and the runner blade. For the guide vane, the positive pitch angle is defined as counterclockwise when viewed from above. In contrast, for the runner blade, the positive pitch angle is defined as clockwise when viewed from above.

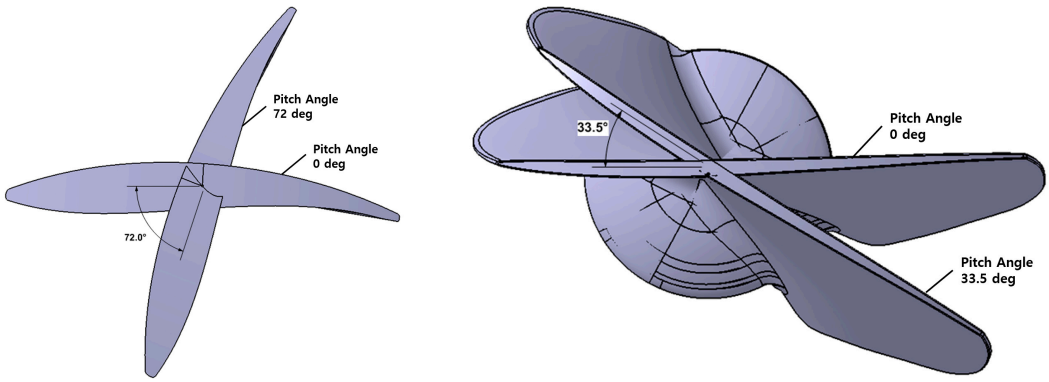


Figure 2. Definition of the pitch angle: (**a**) guide vane; (**b**) runner blade.

3.2. Mesh Generation

Figure 3 presents the three-dimensional grid domain and applied boundary conditions for analyzing the performance of the runner blade. Additionally, the internal interface boundary conditions were applied between the front inlet, central rotating section, and rear outlet to capture the rotational effect in the central rotating section. The rotating area, containing the runner blade within the internal interfaces, was designated as the rotating region, while the front and rear waterways, as well as duct regions, were set as non-rotating regions. In the presenting CFD model, flow analysis was conducted by setting mass flow

rates at the inlet and outlet. At the inlet, the water level remains nearly constant, allowing for a fixed mass flow rate. However, at the outlet, the water level changes continuously, as with tidal fluctuations, necessitating improvements to the existing flow analysis model. To address this, a CFD model was developed with a free surface area behind the outlet to simulate varying outlet water levels, as shown in Figure 4. This free surface area takes the form of a rectangular parallelepiped, and the flow analysis model includes this area.

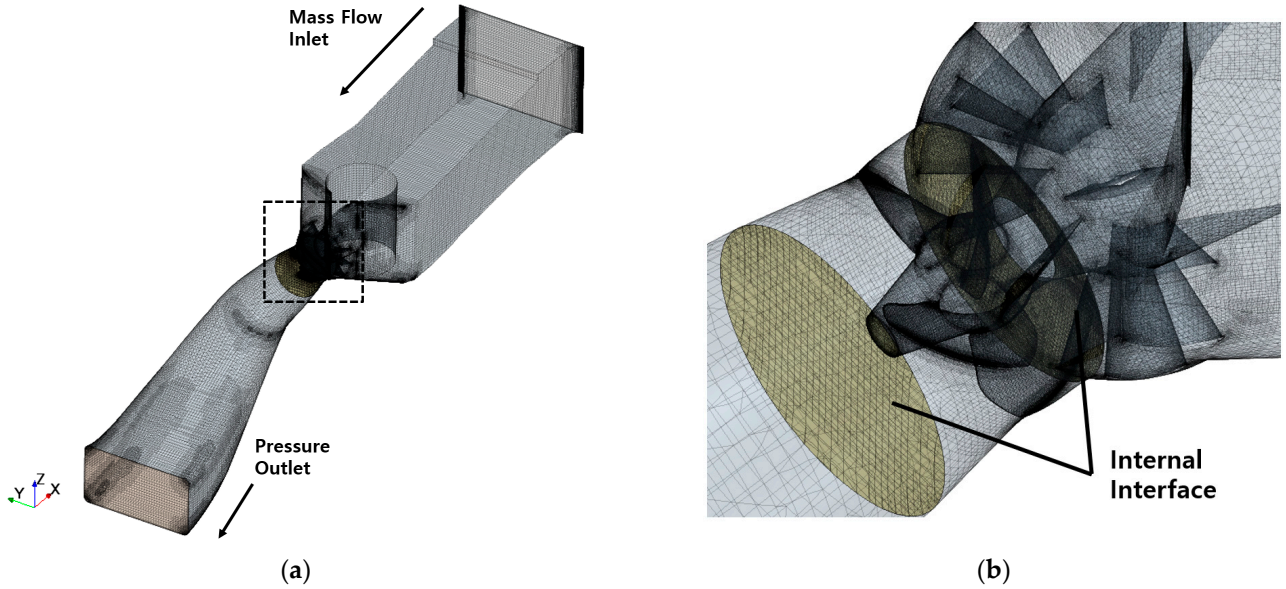


Figure 3. Baseline mesh: (**a**) boundary conditions of the hydropower turbine system; (**b**) internal interface condition between the inlet, rotating, and discharge sections.

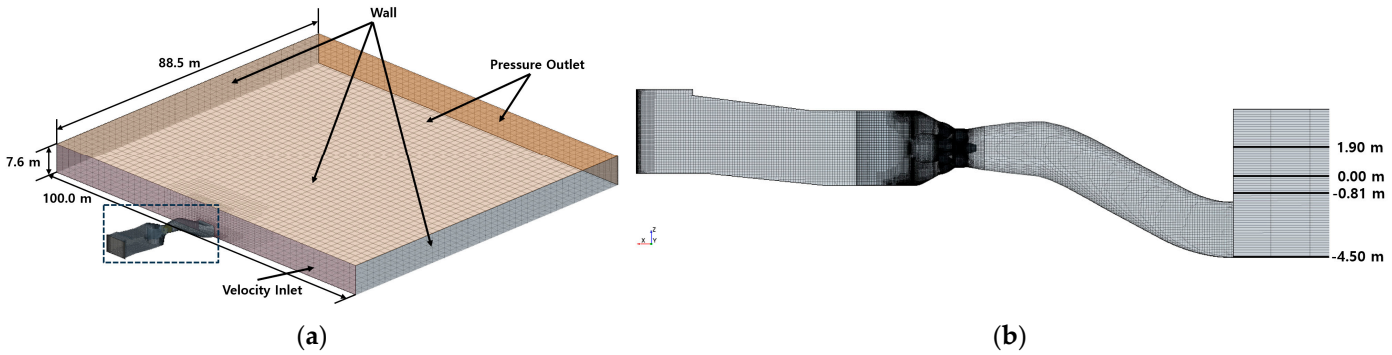
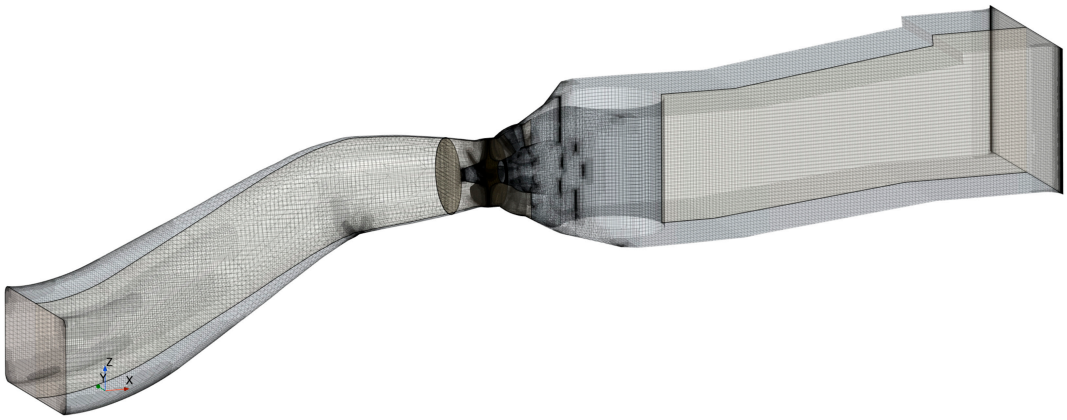


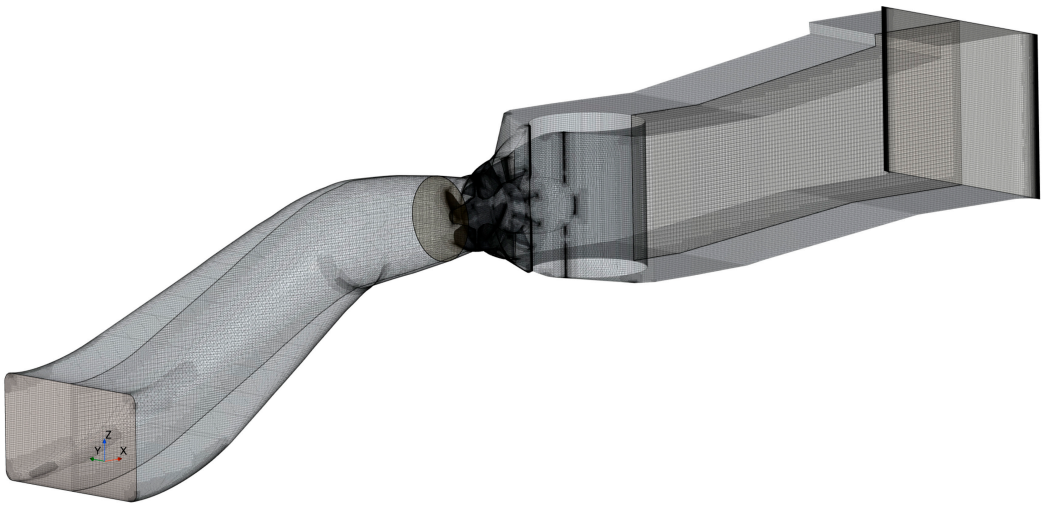
Figure 4. Three-dimensional CFD analysis model with free surface: (**a**) dimension and boundary condition of the free surface model; (**b**) definition of outlet water level for CFD analysis considering free surface effect.

Figure 4 depicts the dimensions and boundary conditions of the free surface area. The grid size and boundary conditions for the pipe region, excluding the rear of the draft tube, were maintained as in the previous model. The dimensions of the free surface area are $88.5 \times 100.0 \times 7.6$ m (length, width, and height), with wall, velocity inlet, and pressure outlet boundary conditions applied. Additionally, to perform flow analysis using the free surface model, the outlet water levels for low- and high-tide conditions were defined. The height of the rear floor at the outlet was set to -4.5 m, establishing water levels of -0.81 m and 1.9 m to simulate low- and high-tide conditions, respectively.

To examine grid convergence, CFD grids with different cell sizes and density distributions were generated and utilized for comparative analysis as shown in Figures 5 and 6. Figure 5 shows full view of entire mesh domain, and Figure 6 presents an enlarged view around the runner blade under four different mesh density conditions. It also illustrates the boundary layer distribution, which accounts for the effects of turbulent viscosity. The baseline mesh (Figures 3a and 6a), which includes seven boundary layers, comprises approximately 5.7 million (5.7 M) unstructured hexahedral elements, with sizes ranging from approximately 0.004 to 0.125 m. The medium mesh (Figures 5a and 6b), with approximately twice the density of the baseline mesh, has 10 boundary layers and a total of approximately 12 million cells. The fine mesh (Figures 5b and 6c), with 10 boundary layers, comprises approximately 33 million cells. Finally, the very fine mesh (Figures 5c and 6d), also with 10 boundary layers, comprises 86 million cells.

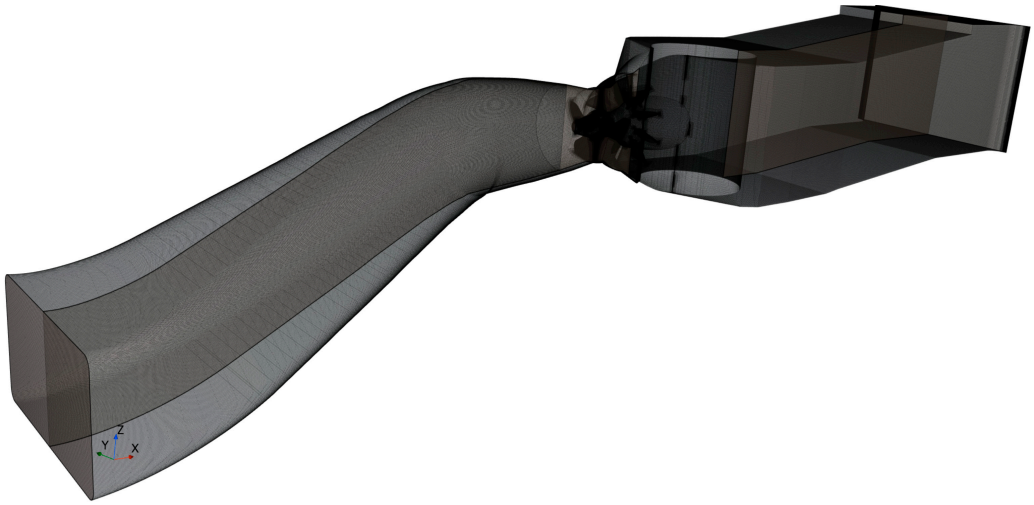


(**a**)



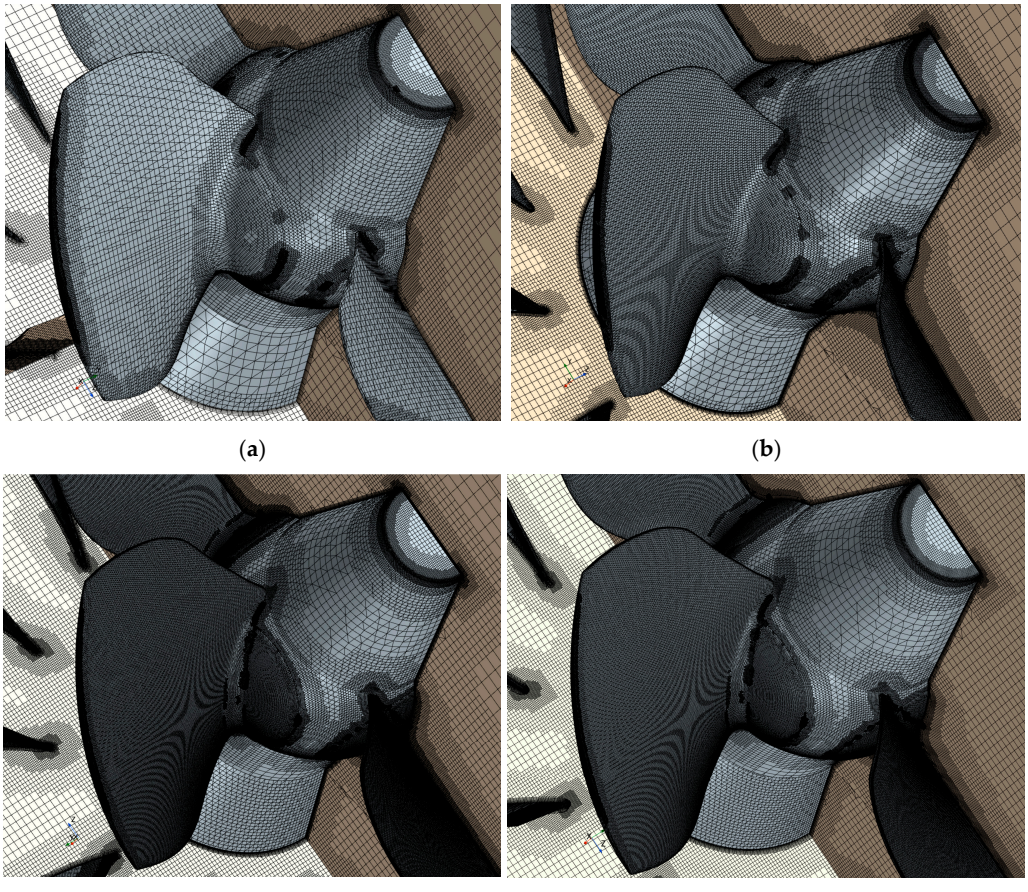
(**b**)

Figure 5. *Cont.*



(**c**)

Figure 5. Three-dimensional CFD analysis meshes (full view): (**a**) medium mesh, 12 M cells; (**b**) fine mesh, 33 M cells; (**c**) very fine mesh, 86 M cells.



(**a**) (**b**)

(**c**) (**d**)

Figure 6. Three-dimensional CFD analysis meshes (enlarged view): (**a**) baseline mesh, 5.7 M cells; (**b**) medium mesh, 12 M cells; (**c**) fine mesh, 33 M cells; (**d**) very fine mesh, 86 M cells.

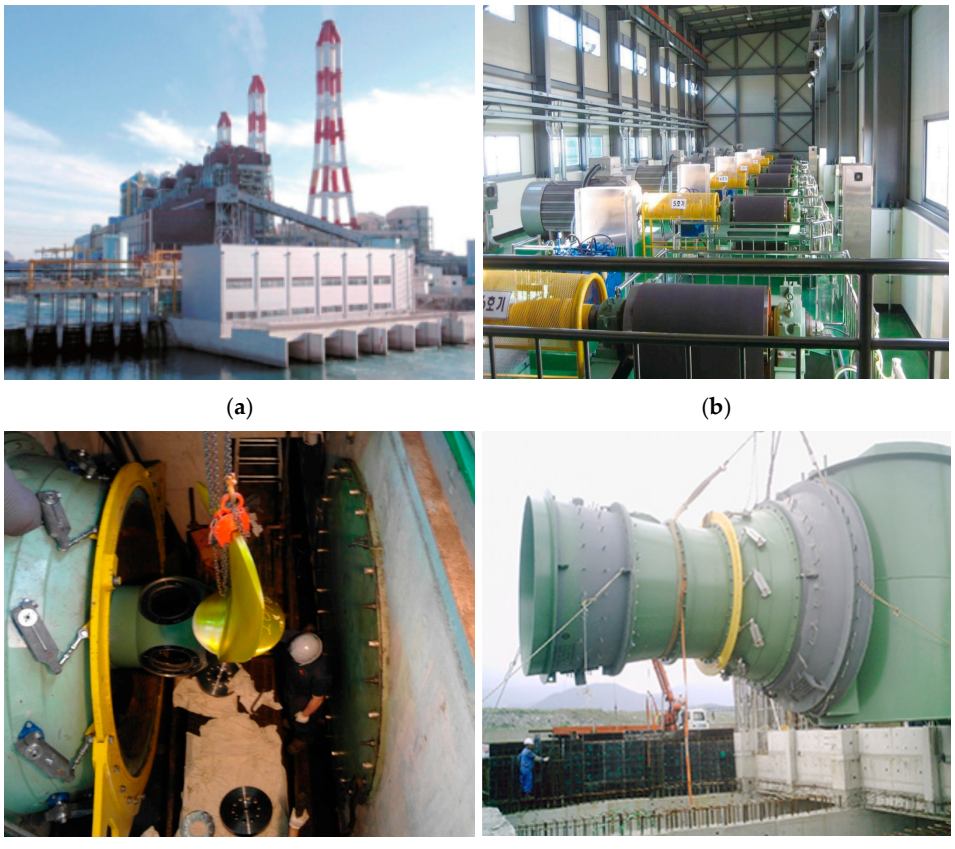
4. Results and Discussion

4.1. Field Test Facility (Korea South-East Power Co.)

This section explains the source of the field test data presented in this study. The Korea South-East Power Co. (KOEN) in Jinju, South Korea operates a total of six 1 MW marine

hydropower systems. These generators utilize the continuously flowing cooling discharge water from a nearby thermal power plant and the tidal difference to generate electricity. The power plant is located in Goseong-gun, Gyeongsangnam-do, South Korea. The system works by trapping the discharge water used as cooling water for the thermal power plant in a dam, utilizing the resulting water head to drive turbines and generate electricity. This facility is the largest small hydropower plant in South Korea. The expected annual power production of the KOEN marine hydropower system is about 23 GWh, which is enough to supply clean, emission-free electricity to approximately 7600 households.

Figure 7 shows an overview of the KOEN marine hydropower system and its main components. Figure 5a displays the marine hydropower system building located along the coast to utilize the cooling discharge water from the thermal power plant. Figure 5b presents a photograph of the electric generator drive unit housed within the building. Key mechanical components, such as the duct, turbine, and control system for hydropower generation, are installed in the basement of this building. Additionally, the building is equipped with an operation control and monitoring room, where the optimal vane and runner blade angles are controlled according to the inlet flow rate and tidal fluctuations to achieve maximum power generation through the maximum power point tracking (MPPT) method. There is also a dedicated control room for monitoring the 24 h equipment operation status, power generation, and data storage. The inlet flow rate, which varies according to the operating status of the thermal power plant, the seawater level at the discharge outlet due to tidal fluctuations, and various types of operational data, is recorded in real time. Using the provided monitoring software, users can extract operational data for any desired time period.



(**a**) (**b**)

(**c**) (**d**)

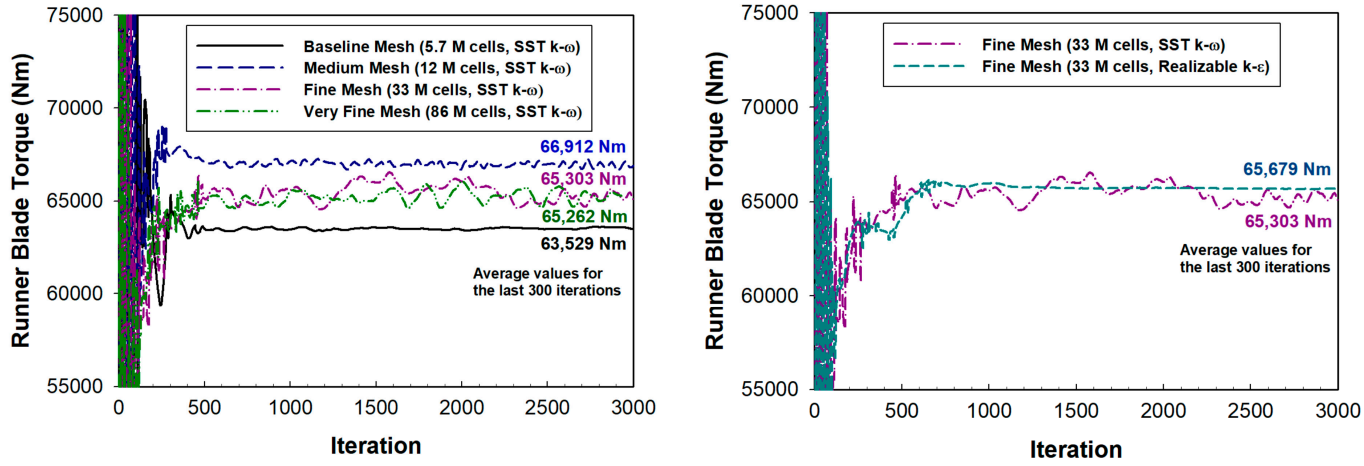
Figure 7. KOEN 1 MW marine hydropower system: (**a**) panoramic view (Total 6 MW, 1 MW × 6 units); (**b**) electric generator drive units; (**c**) underground located blade, hub, and duct parts; (**d**) separated main rotor-duct unit.

4.2. CFD Analysis for the Maximum Output Condition

In this study, a performance analysis of the hydropower turbine system was conducted by selecting the maximum output condition as the initial flow analysis scenario. To mirror the actual hydropower turbine system, the pitch angles of the guide vane and runner blade were set to 72.0° and 33.5°, respectively. The flow rate at the inlet was set to 21.67 m^3/s, and since the inlet water level remained nearly constant, an inlet mass flow rate of 22,211.75 kg/s was used, calculated by multiplying the flow rate by the seawater density of 1025 kg/m^3. The same mass flow rate condition was applied to the pressure outlet located at the rear of the discharge section. The steady flow analysis for this condition was first conducted to evaluate the impact of CFD mesh density. Various analyses were performed using three different mesh configurations, namely the baseline mesh (5.7 M cells), medium mesh (12 M cells), fine mesh (33 M cells), and very fine mesh (86 M cells).

Figure 8 and Table 1 illustrate the variation in blade torque during the convergence history for four different mesh densities, as obtained from flow analysis using the MRF method (previously described in Section 3.1). The blade rotation speed was 141.7 rpm, and all boundary conditions were identical to those described earlier. From 2500 iterations onward, all mesh models exhibited a converged trend. In case of the medium, fine, and very fine mesh models, slight numerical perturbations were observed even in the convergence region due to the transient characteristic of the SST k-ω turbulence model. The number displayed on the far-right side of the graph represents the average blade torque calculated over the final 300 iterations. The power prediction results for the runner blade under different grid densities show a maximum difference of approximately 5%. However, in the case of the fine mesh and very fine mesh, the difference was about 0.07%, indicating that these grids can be considered to have achieved full convergence. Table 1 compares the power levels obtained from KOEN's field test results and the predictions from CFD analysis, with the differences presented as numerical data. The field test results represent the 1 min average of net power values, which inherently include mechanical and electrical losses. The power predicted by the CFD analysis was calculated by multiplying the average torque by the rotational speed, which corresponds to the shaft power without accounting for losses. Therefore, considering these losses, it is more reasonable for the power predicted by the CFD analysis to slightly overestimate the actual field test values. The server computer used for the comparative analysis in Figure 8 is equipped with two AMD EPYC 7763 64-core processors and 1024 GB of memory. For reference, the computation time for 3000 iterations of the fine mesh model, which contains approximately 33 million cells, was about 240 min (4 h).

Additionally, to briefly assess the effect of different CFD, the turbulence model realizable k-ε was also applied to the fine mesh. Figure 8b compares the analysis results obtained using the realizable k-ε turbulence model with those from the SST k-ω model. Excluding the fluctuation characteristics of the SST k-ω model, the quantitative power prediction values presented in Table 1 show a difference of only 0.59%, confirming that the results are nearly identical. A more comprehensive evaluation of the effects of various turbulence models is beyond the primary scope of this paper. Such an evaluation, particularly from the perspective of dynamic loads acting on the blade, will be conducted in future studies. Despite primarily utilizing the SST k-ω turbulence model in this study, from the perspective of performance analysis of hydropower turbines, it seems that the k-ε turbulence model effectively suppresses unnecessary numerical perturbations, making it a highly practical choice. Although the analysis of dynamic loads acting on the blade is not directly related to the main focus of this study, another reason for applying the SST k-ω turbulence model in this study is to facilitate future extensions of extreme design load and fatigue load analyses.



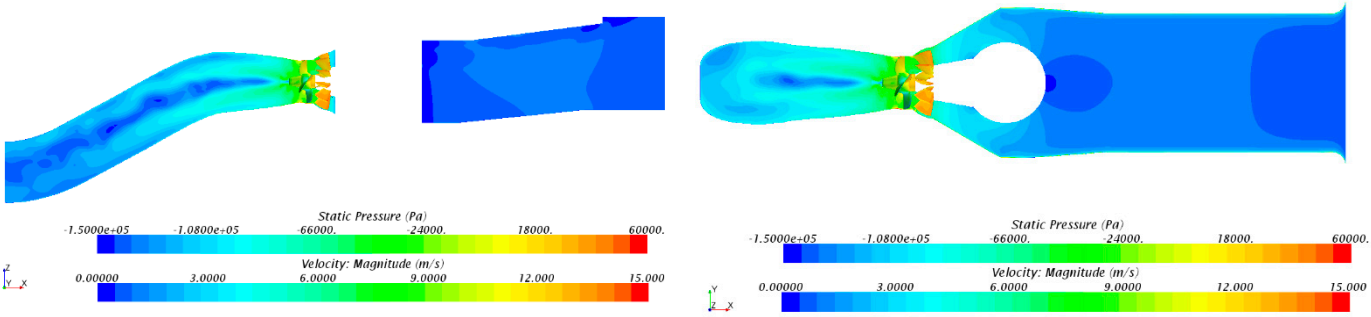
(**a**) (**b**)

Figure 8. Comparison of runner blade torque variation according to changes in mesh density and turbulence model: (**a**) effect of mesh density; (**b**) effect of turbulence model.

Table 1. Comparison between the CFD analysis and measured performance data at 141.7 rpm.

	Flow Rate	Head	Output	Difference
	m^3/s	m	kW	%
Field Test (KOEN)	21.67	4.93	938.0	-
CFD (SST k-ω, Baseline mesh)	21.67	-	942.7	0.50
CFD (SST k-ω, Medium mesh)	21.67	-	992.9	5.85
CFD (SST k-ω, Fine mesh)	21.67	-	969.0	3.31
CFD (Realizable k-ε, Fine mesh)	21.67	-	974.6	3.90
CFD (SST k-ω, Very fine mesh)	21.67	-	968.4	3.24

Figure 9 shows the surface pressure distribution on the designed runner blade and guide vane as well as the velocity distribution within the pipeline. A relatively high flow velocity was observed at the blade tip, influenced by the wake generated behind the hub as the flow passes through the runner blade and the gap between the blade tip and pipeline. Additionally, the blade tip surface showed a relatively low pressure distribution due to the impact of the wake vortex. Examining the surface pressure and pipeline velocity distribution at the top of the hydropower turbine system revealed an increase in flow velocity at the constriction point in front of the runner blade.



(**a**) (**b**)

Figure 9. Static pressure and velocity distributions at maximum output conditions: (**a**) side view; (**b**) top view.

The results presented in this study represent only a small portion of the numerous CFD analysis results we have conducted before under various conditions to enhance

the performance and efficiency of hydropower turbines using CFD techniques. From an academic perspective, it would be ideal to perform all analyses using the fine mesh model presented earlier. However, from a practical standpoint that considers both design and analysis efficiency, utilizing the baseline mesh level is more advantageous. Even with an difference margin of approximately 5%, using the baseline mesh significantly reduces the computational time required for CFD analysis, enabling the analysis and evaluation of a larger number of design conditions. Considering the larger and more extensive CFD analyses presented in the latter part of this paper, the baseline mesh level proves to be a more practical approach. It allows for efficient utilization of computational resources while maintaining a reasonable level of accuracy.

4.3. Unsteady CFD Analysis for Different Tide Conditions

Based on data measured in the control room of the actual hydropower turbine system, the date with the highest recorded values was selected for performance analysis under both low- and high-tide conditions. Table 2 presents the tide and outlet water-level data over a specific period, with performance analysis conducted on Day 8 during low and high tides, when the outlet water-level difference reached its peak at 2.71 m. In an actual hydropower turbine system, the opening rate of the guide vane can be monitored in real time. For the runner blades, the pitch angle adjusts in conjunction with the guide vane. In the flow analysis model, the guide vane's opening rate was calculated such that a pitch angle of 0° corresponded to an opening rate of 0%, and a pitch angle of 90° corresponded to an opening rate of 100%. Following this approach, the pitch angles of the guide vane and runner blade were set to 69.2° and 34.5°, respectively, during low tide and 80.7° and 38.2°, respectively, during high tide.

Table 2. Outlet water lever data for CFD analysis.

Date	Outlet Water Level at Low Tide	Outlet Water Level at High Tide	Outlet Water Level Between Low- and High-Tide Conditions
	m	m	m
Day 01	−0.43	0.87	1.30
Day 02	−0.44	0.73	1.17
Day 03	−0.52	0.91	1.43
Day 04	−0.57	1.09	1.66
Day 05	−0.68	1.42	2.10
Day 06	−0.75	1.57	2.32
Day 07	−0.80	1.71	2.51
Day 08	−0.81	1.90	2.71
Day 09	−0.78	1.88	2.66
Day 10	−0.79	1.79	2.58
Day 11	−0.70	1.67	2.37
Day 12	−0.62	1.36	1.98
Day 13	−0.55	1.08	1.63
Day 14	−0.35	0.68	1.03
Day 15	−0.34	0.59	0.93

For low- and high-tide conditions, unsteady CFD analyses were performed using the MRF method for three different mesh density models. Figure 10a illustrates the variation in runner blade torque over time under the low-tide condition, while Figure 10b presents the result for the high-tide condition. To achieve rapid convergence, a variable time-step size was applied, with five sub-iterations per time step. The values shown on the right side of the graph represent the average torque during the final one second of the simulation. The server computer used was equipped with two AMD EPYC 7763 64-core

processors and 1024 GB of memory. The computation time for 5 s of simulation using the baseline mesh (5.7 M cells) was 115 min (1.9 h), while that using the fine mesh model (33 M cells) was approximately 700 min (11.7 h). Figure 11 illustrates the streamlines for the low- and high-tide conditions. The streamline patterns in the region from the inlet to the runner blade appeared almost identical for both cases; however, the velocity of the flow entering the runner blade differed due to the head difference, with the low-tide condition exhibiting a higher velocity. Downstream of the runner blade, the streamlines showed swirl phenomena caused by the rotational effect, with the low-tide condition displaying stronger swirl characteristics in the wake region compared to the high-tide condition.

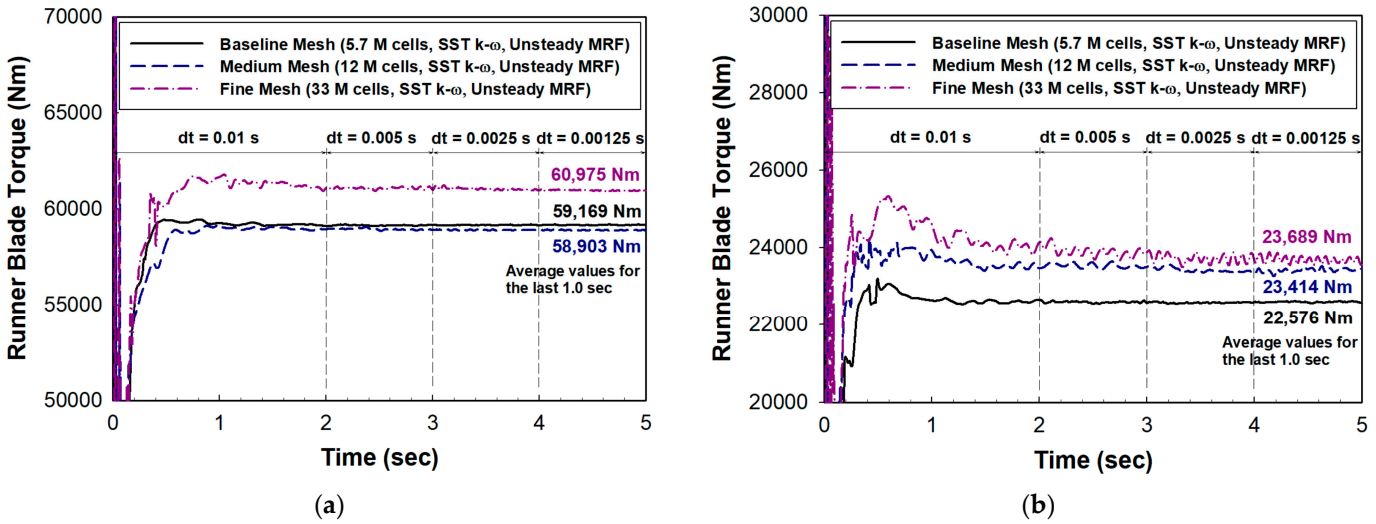


Figure 10. Comparison of unsteady runner blade torque variation according to changes in mesh density for high and low tide conditions: (**a**) low-tide condition; (**b**) high-tide condition.

Table 3 presents a comparison between the actual measurement results and the flow analysis results of the hydropower turbine system the low- and high-tide conditions without the free surface model. As before, the field test results represent the 1 min average of net power values, which inherently include mechanical and electrical losses. The power predicted by the CFD analysis was calculated by multiplying the average torque by the rotational speed, which corresponds to the shaft power without accounting for any loss effects. For the baseline mesh, the differences compared to the field test results were 1.62% for the low-tide condition and 0.9% for the high-tide condition. In the case of the medium mesh, the differences were 1.16% for the low-tide condition and 4.65% for the high-tide condition. For the fine mesh, the differences were 4.72% for the low-tide condition and 5.88% for the high-tide condition. As previously explained, since the field test results represent net power values that account for losses, the fine mesh results are more accurate when considering system losses of approximately 5% or higher. However, the fine mesh required a computational time approximately six times longer than the baseline mesh.

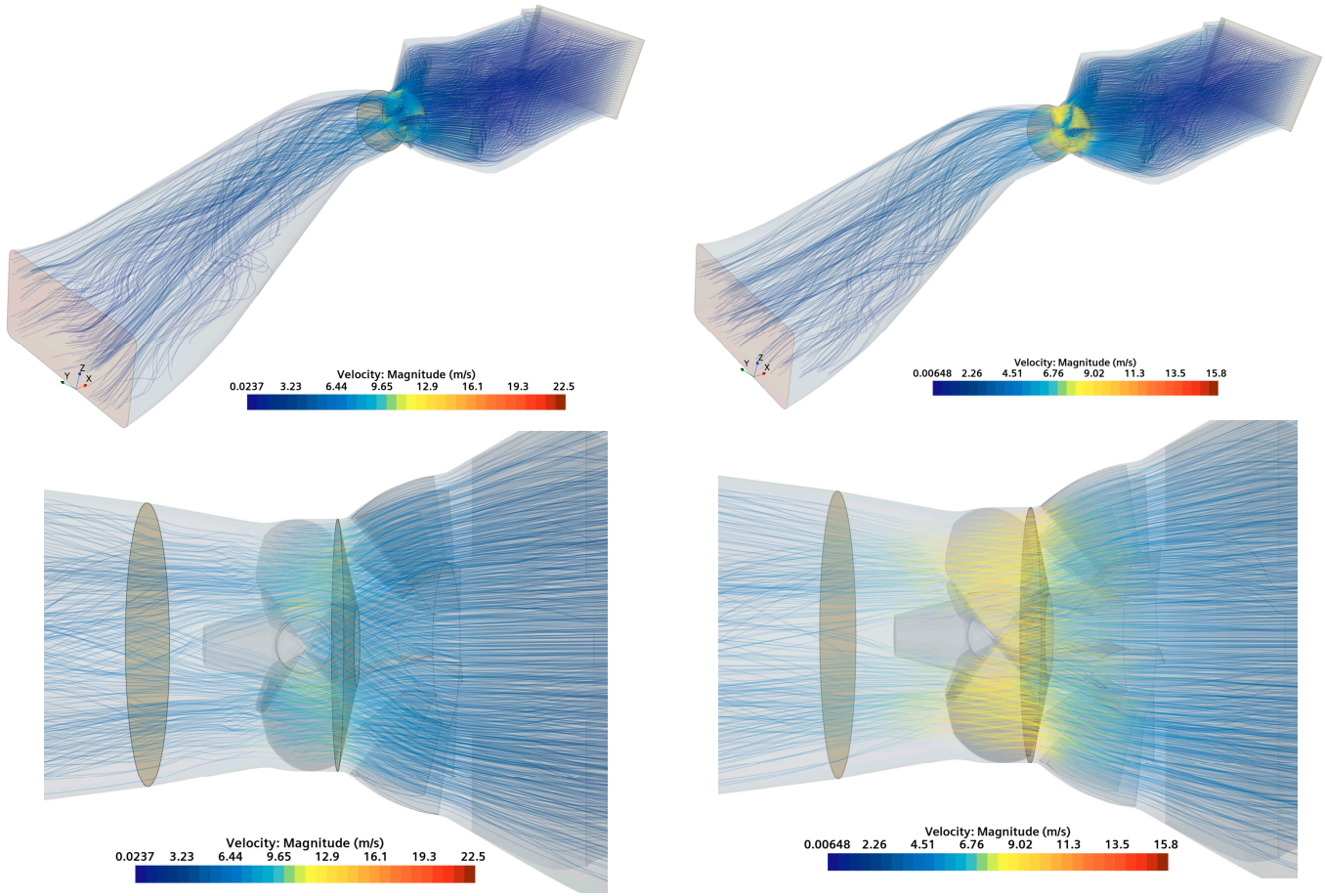


Figure 11. Streamline plots with velocity magnitude under different tide conditions: (**a**) low-tide condition; (**b**) high-tide condition.

Table 3. Comparison of field test and CFD analysis results under varying tide conditions.

Tide Conditions		Opening Ratio	Guide Vane Pitch Angle	Runner Blade Pitch Angle	Generator Output	Difference %
		%	deg	deg	kW	
Low tide	Field Test (KOEN)	76.83	-	-	864	-
	CFD (SST k-ω, Baseline mesh)	76.83	69.2	34.5	877.9	1.62
	CFD (SST k-ω, Medium mesh)	76.83	69.2	34.5	874.1	1.16
	CFD (SST k-ω, Fine mesh)	76.83	69.2	34.5	904.8	4.72
High tide	Field Test (KOEN)	89.65	-	-	332	-
	CFD (SST k-ω, Baseline mesh)	89.65	80.7	38.2	335.0	0.90
	CFD (SST k-ω, Medium mesh)	89.65	80.7	38.2	347.4	4.65
	CFD (SST k-ω, Fine mesh)	89.65	80.7	38.2	351.6	5.88

4.4. Unsteady CFD Analysis Using a Free Surface Model

Finally, unsteady flow analyses using the MRF method were also conducted with the free surface model under the same low- and high-tide water levels as before. To enhance the approach of applying a uniform mass flow rate at the outlet, the actual outlet water level was implemented using a second-order volume of fluid (VOF) wave model. A flat wave condition was applied, with water levels for the low- and high-tide conditions set as initial conditions. To account for the multiphase flow of air and water, a multiphase flow interaction condition was applied, with the densities of air and seawater set to 1.225 kg/m^3

and 1025 kg/m^3, respectively. The pitch angles of the guide vane and runner blade were kept consistent with those in the previous flow analysis.

The analysis for these conditions required significantly more computational time compared to the previous conditions. Therefore, only baseline mesh and medium mesh analyses were performed. The baseline mesh with the free surface included is similar to that in Figure 4a and consists of 6.1 million cells. Similarly, the medium mesh with the free surface included corresponds to Figure 12 and comprises 14.8 million cells. Notably, the regions excluding the free surface area have a grid density similar to the medium mesh presented in Figures 5 and 6. To achieve rapid convergence, a variable time-step size was also applied, with five sub-iterations per time step.

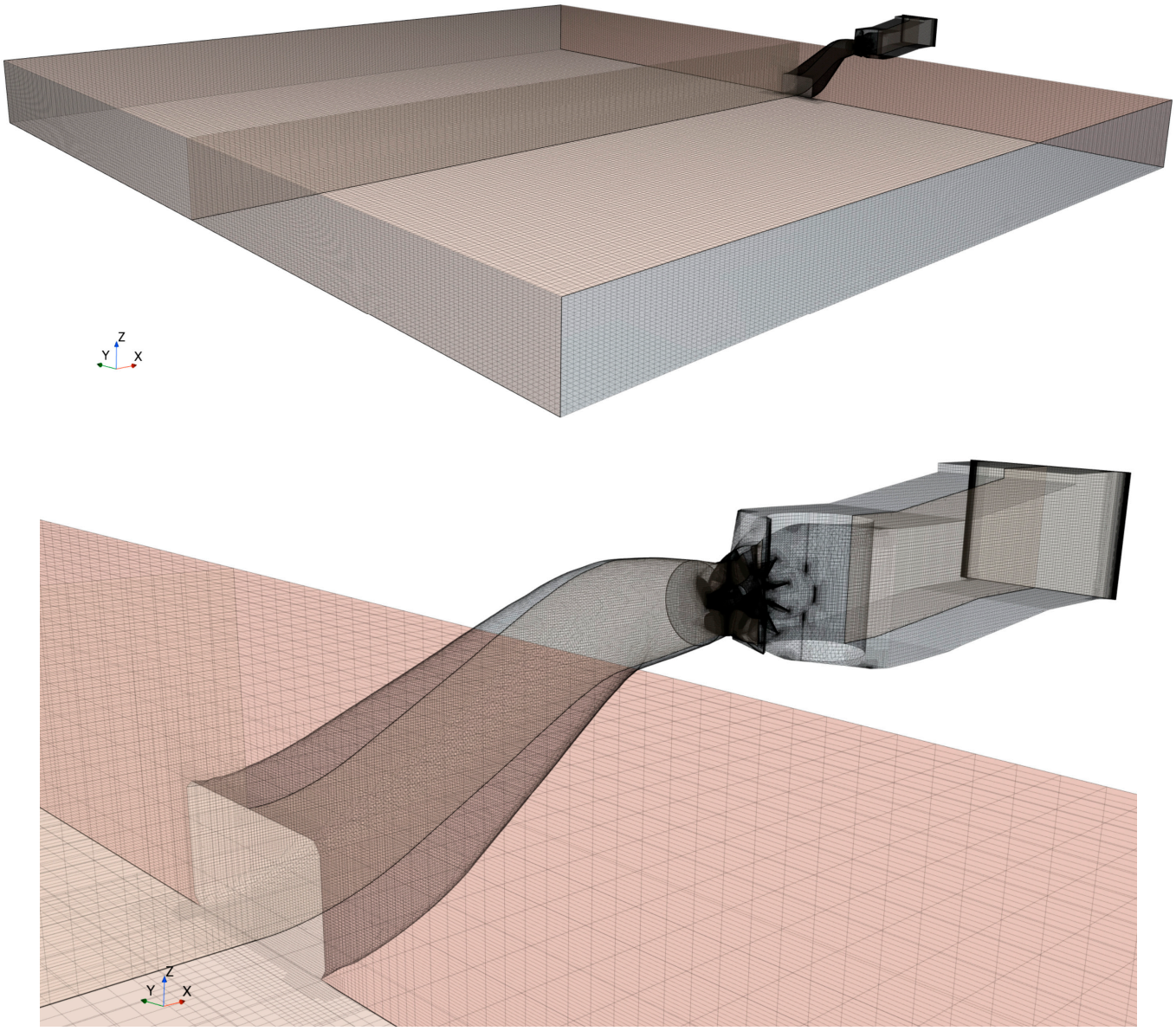
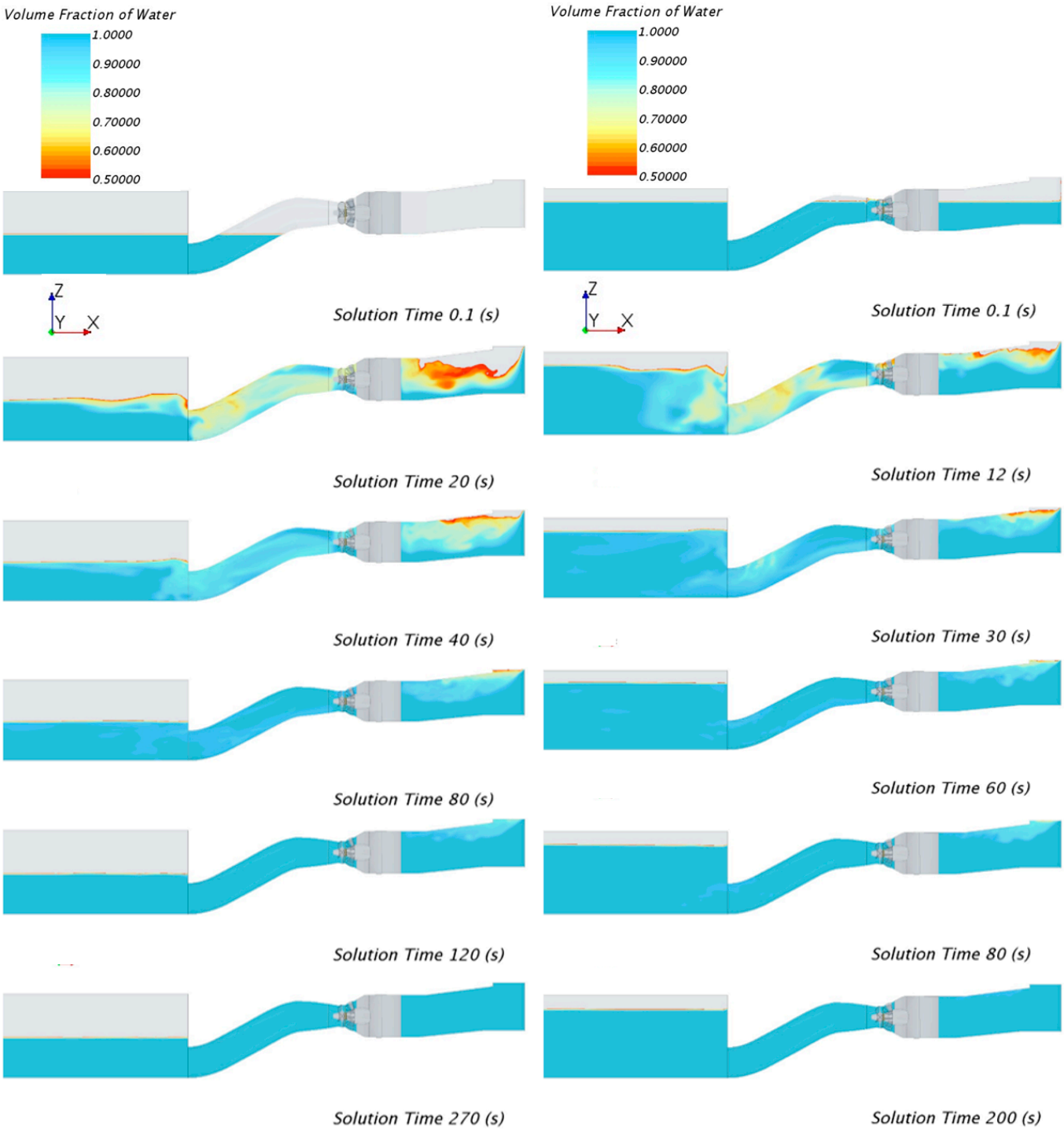


Figure 12. Three-dimensional mesh for free surface model: medium mesh (14.8 M cells).

Figure 13 shows the unsteady CFD analysis results for low- and high-tide conditions with the free surface model, showing the seawater flow over time. Under low-tide conditions, the pipeline initially contains almost no water. After approximately 20 s, seawater flows through the runner blade, filling the rear discharge area, and by around 120 s, the pipeline is fully filled with water. In contrast, under high-tide conditions, the pipeline

begins more than half filled. Seawater reaches the rear discharge area after about 12 s, and by 80 s, the pipeline is completely filled with seawater. In the CFD analysis with the free surface model, time is required for seawater to fill the pipeline, causing the analysis results to remain unconverged while the water level is changing. However, once the pipeline is fully filled, the analysis results converge. With the free surface model, significantly more time was required compared to the existing flow analysis conditions.



(**a**) (**b**)

Figure 13. The simultaneous water flow behavior with free surface model with respect to time: (**a**) low-tide condition; (**b**) high-tide condition.

For the analysis considering the free surface effect, Figure 14 presents the time-dependent variation in blade torque from the moment the inlet gate opens until a converged torque value is reached. In this analysis, a variable time-step was also applied, and the variations in Δt for the low- and high-tide conditions are shown in the enlarged view on the right. For the baseline mesh, the influence of time-step reduction was minimal, and the average torque level remained nearly constant. In contrast, for the medium mesh, when Δt was reduced to 0.00125 s, a slight torque decrease of 1.52% was observed for the low-tide condition, while a 1.65% torque decrease was noted for the high-tide condition. This behavior is attributed to the sensitivity of the VOF model to grid density in the free surface region. In the flow analysis considering low- and high-tide conditions without the free surface model in Section 4.2, results converged quickly within 5 s of physical time. However, with the free surface model, the initial conditions assumed an empty pipe, requiring water to enter from the inlet. As a result, convergence was delayed until the pipe filled, leading to very longer simulation times.

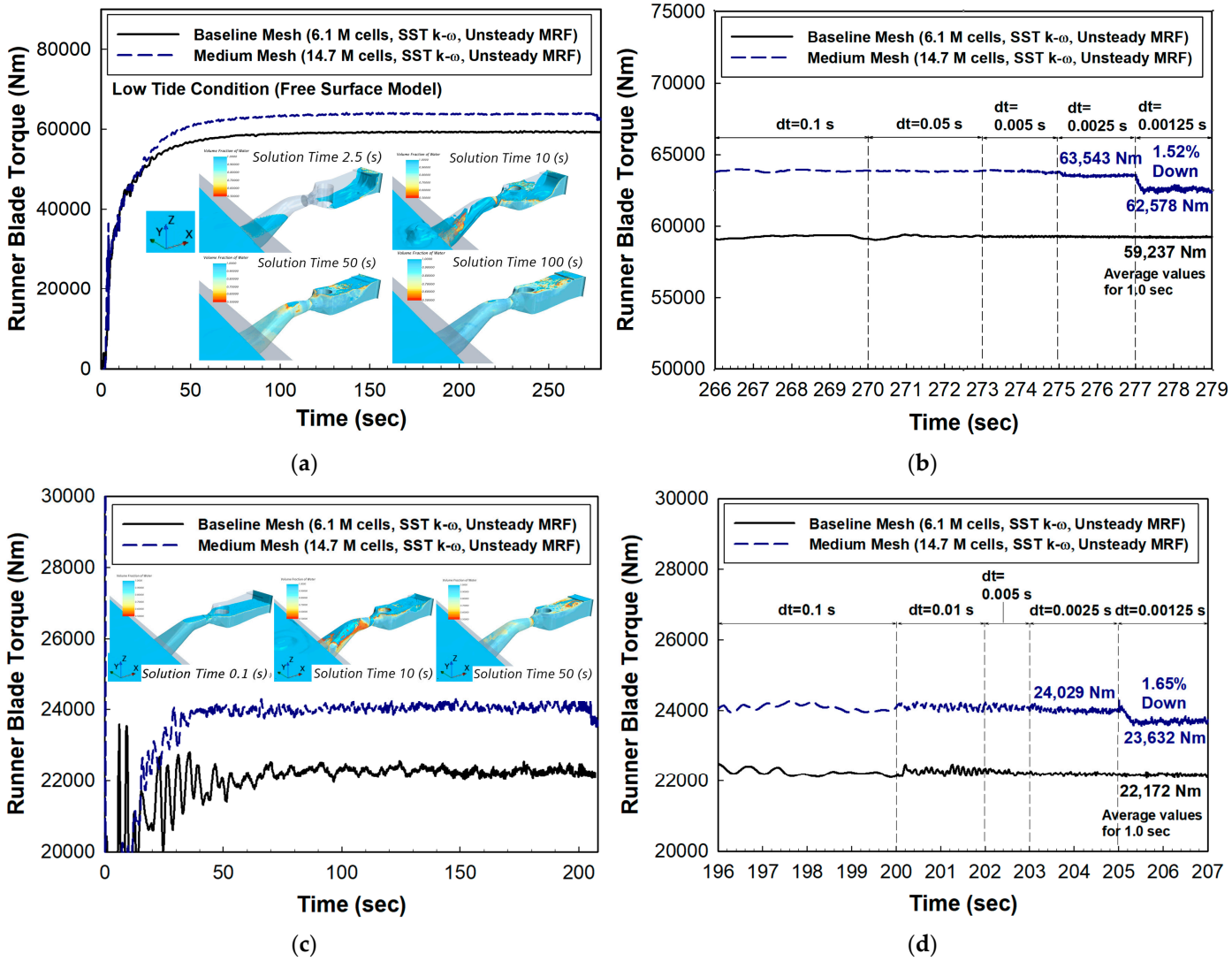


Figure 14. Comparison of unsteady runner blade torque variation according to changes in mesh density for free surface models: (**a**) low-tide condition; (**b**) low-tide condition (enlarged view); (**c**) high-tide condition; (**d**) high-tide condition (enlarged view).

Table 4 presents the comparison between actual measurement data and flow analysis results using the free surface model. As before, the field test results represent the 1 min

average of net power values, which inherently include mechanical and electrical losses. As in the previous cases, the power predicted by the CFD analysis was calculated by multiplying the average torque by the rotational speed, which corresponds to the shaft power without accounting for any loss effects. For the free surface baseline mesh (6.1 M cells), the results showed a 1.74% increase in power compared to the field test under the low-tide condition and a 0.9% decrease under the high-tide condition. Meanwhile, the free surface medium mesh (14.8 M cells) showed a 7.47% higher power prediction for the low-tide condition and a 5.62% higher prediction for the high-tide condition. As previously explained, considering the effects of mechanical and electrical losses, predicting higher power than the field test results is a more reasonable outcome. However, at this stage, we must also consider computational efficiency, as the typical design process requires extensive flow analyses under a wide variety of conditions. Figure 15 presents a comparison graph of the computational time required for flow analyses using the free surface model with two different grid density levels. The total number of cells in the medium mesh is approximately 2.43 times greater than that of the baseline mesh. However, the computational time required for the time-response analysis increased by approximately eight times. The significant increase in computational time, exceeding the proportional grid density ratio, is attributed to the additional time required for the VOF model analysis due to the higher grid density as well as the substantially increased data exchange time in shared memory process (SMP) parallel computation. Notably, in such unsteady flow analyses, it is important to highlight that a considerable amount of time is also spent in the final stage of achieving convergence, where the time step is progressively reduced during the last few seconds of the simulation to obtain a fully converged solution.

Table 4. Comparison of field test and CFD analysis results with free surface model.

Tide Conditions (Free Surface Model)		Opening Ratio	Guide Vane Pitch Angle	Runner Blade Pitch Angle	Generator Output	Difference %
		%	deg	deg	kW	
Low tide	Field Test (KOEN)	76.83	-	-	864	-
	CFD (SST k-ω, Baseline mesh)	76.83	69.2	34.5	878.9	1.74
	CFD (SST k-ω, Medium mesh)	76.83	69.2	34.5	928.6	7.47
High tide	Field Test (KOEN)	89.65	-	-	332	-
	CFD (SST k-ω, Baseline mesh)	89.65	80.7	38.2	329.1	−0.90
	CFD (SST k-ω, Medium mesh)	89.65	80.7	38.2	350.7	5.62

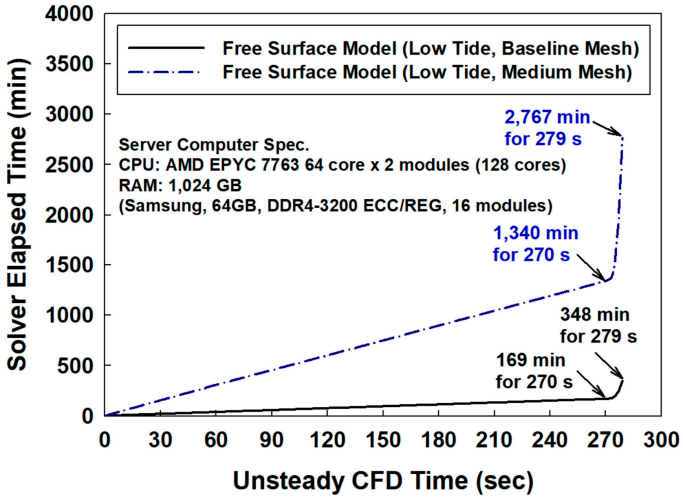


Figure 15. The time required for the unsteady flow analysis of the free surface model (with 128-core parallel processing, low-tide condition).

The reason for constructing the free surface analysis model was to evaluate the level of impact of dynamic loads on the blades during the restart of the hydro power turbine system following annual overhauls and to identify mitigation strategies during operation. The performance analysis was conducted solely to determine the deviation level compared to the non-free surface model. Since the differences in results were negligible, the non-free surface model can be considered more efficient from a performance analysis perspective. Interestingly, in the case of the 1 MW hydro power turbine system considered in this study, the baseline mesh analysis results closely matched the net power results from the field test, even without accounting for the effects of mechanical and electrical losses in the system. Furthermore, based on the current analyses and comparison of results across various grid density conditions, the baseline mesh presented in this study can be considered practically suitable for use in the design process, where efficient evaluation of various factors and effects on the hydropower turbine system is required.

5. Conclusions

In this study, a three-dimensional computational fluid dynamics (CFD) analysis was conducted to evaluate the flow and performance of a 1 MW hydropower turbine system. Steady and unsteady incompressible viscous flow analyses, utilizing the SST k-ω turbulence model and the MRF method to account for the rotational effect of the runner blade, were performed with various grid densities to evaluate grid convergence. In addition to applying numerical outlet boundary conditions, an analysis incorporating the free surface effect at the outlet—consistent with actual operating conditions—was conducted, and its impact was examined. The CFD results closely matched the actual field measurements, leading to the following conclusions. The grid density levels used in this study ranged from 5.7 M cells (baseline mesh) to 86 M cells (very fine mesh) for the maximum power condition. For the non-free surface model, a fine mesh with 33 M cells was employed, while for the free surface model, a medium mesh with 14.7 M cells was used. Across all conditions predicted using the same SST k-ω turbulence model with different grid densities, the deviation in shaft power was within a maximum of 5.7%. For all conditions, the shaft power predicted by the baseline mesh model, which did not account for mechanical and electrical losses, was nearly identical to the field test results that included these losses. In contrast, denser meshes predicted shaft power values approximately 3–5% higher, showing closer alignment with the field test results when loss effects were considered. The difference in power prediction results between considering and not considering the free surface effect at the outlet revealed that, for the low-tide condition, the baseline mesh exhibited a 0.12% difference, while the medium mesh showed a 6.31% difference. For the high-tide condition, the baseline mesh exhibited a 1.8% difference, while the medium mesh showed a 0.97% difference. These findings suggest that the influence of mesh density is more pronounced in the low-tide condition when the free surface effect is considered. The flow analysis and performance evaluation methods for hydropower turbine systems presented in this study are anticipated to contribute to enhancing performance predictions and assessing extreme design loads, thereby aiding in the development of high-efficiency hydropower turbine systems in the future.

Author Contributions: Authors K.-H.K., D.-H.K. and S.-J.H. are responsible for generating the CFD models; conducting the initial, updated, and revised analyses; and drafting the paper. Authors D.-H.K. and S.-M.L. provided valuable advice on the used methodology and field test, evaluated the results, and performed critical proofreading and review. All authors have read and agreed to the published version of the manuscript.

Funding: This work was supported by the Gyeongsang National University Fund for Professors on Sabbatical Leave, 2024.

Data Availability Statement: The raw data supporting the conclusions of this article will be made available by the authors on request.

Acknowledgments: The field test data were obtained from the facilities of Korea South-East Power Co., South Korea. The authors would like to express their gratitude for the provision of actual field test data.

Conflicts of Interest: Author Sang-Myung Lee was employed by the Korea South-East Power Co. (KOEN). The remaining authors declare that the research was conducted in the absence of any commercial or financial relationships that could be construed as a potential conflict of interest.

References

1. Tiwari, G.; Kumar, J.; Prasad, V.; Patel, V.K. Utility of CFD in the design and performance analysis of hydraulic turbines—A review. *Energy Rep.* **2020**, *6*, 2410–2429. [CrossRef]
2. Abeykoon, C. Modelling and optimization of a Kaplan turbine—A comprehensive theoretical and CFD study. *Clean. Energy Syst.* **2022**, *3*, 100017. [CrossRef]
3. Kaniecki, M.; Krzemianowski, Z.; Banaszek, M. Computational Fluid Dynamics Simulations of Small Capacity Kaplan Turbines. *Trans. Inst. Fluid-Flow Mach.* **2011**, *123*, 71–84.
4. Akinyemi, O.S.; Liu, Y. CFD Modeling and Simulation of a Hydropower System in Generating Clean Electricity from Water Flow. *Int. J. Energy Environ. Eng.* **2015**, *6*, 357–366. [CrossRef]
5. Liu, K.; Yang, F.; Yang, Z.; Zhu, Y.; Cheng, Y. Runner Lifting-Up during Load Rejection Transients of a Kaplan Turbine: Flow Mechanism and Solution. *Energies* **2019**, *12*, 4781. [CrossRef]
6. Peczkis, G.; Wiśniewski, P.; Zahorulko, A. Experimental and Numerical Studies on the Influence of Blade Number in a Small Water Turbine. *Energies* **2021**, *14*, 2604. [CrossRef]
7. Iovănel, R.G.; Dehkharqani, A.S.; Bucur, D.M.; Cervantes, M.J. Numerical Simulation and Experimental Validation of a Kaplan Prototype Turbine Operating on a Cam Curve. *Energies* **2022**, *15*, 4121. [CrossRef]
8. Demirdzic, I.; Lilek, Z.; Peric, M. A collocated finite volume method for predicting flows at all speeds. *Int. J. Numer. Methods Fluids* **1993**, *16*, 1029–1050. [CrossRef]
9. Demirdzic, I.; Muzaferija, S. Numerical method for coupled fluid flow, heat transfer and stress analysis using unstructured moving meshes with cells of arbitrary topology. *Comput. Methods Appl. Mech. Eng.* **1995**, *125*, 235–255. [CrossRef]
10. Ferziger, J.H.; Peric, M. *Computational Methods for Fluid Dynamics*, 3rd ed.; Springer: Berlin, Germany, 2002.
11. Zhang, G.; Yang, Y.; Chen, J.; Jin, Z.; Dykas, S. Numerical study of heterogeneous condensation in the de Laval nozzle to guide the compressor performance optimization in a compressed air energy storage system. *Appl. Energy* **2024**, *356*, 122361. [CrossRef]
12. Tran, T.T.; Kim, D.H.; Song, J. Computational Fluid Dynamic Analysis of a Floating Offshore Wind Turbine Experiencing Platform Pitching Motion. *Energies* **2014**, *7*, 5011–5026. [CrossRef]
13. Tran, T.T.; Kim, D.H. Fully coupled aero-hydrodynamic analysis of a semi-submersible FOWT using a dynamic fluid body interaction approach. *Renew. Energy* **2016**, *92*, 244–261. [CrossRef]
14. Versteeg, H.K.; Malalasekera, W. *An Introduction to Computational Fluid Dynamics: The Finite Volume Method*; Pearson Education: London, UK, 2007.
15. Abdelghany, E.S.; Sarhan, H.H.; Alahmadi, R.; Farghaly, M.B. Study the Effect of Winglet Height Length on the Aerodynamic Performance of Horizontal Axis Wind Turbines Using Computational Investigation. *Energies* **2023**, *16*, 5138. [CrossRef]

Disclaimer/Publisher's Note: The statements, opinions and data contained in all publications are solely those of the individual author(s) and contributor(s) and not of MDPI and/or the editor(s). MDPI and/or the editor(s) disclaim responsibility for any injury to people or property resulting from any ideas, methods, instructions or products referred to in the content.